Energy 36 (2011) 917–921

Contents lists available at ScienceDirect

Energy

journal homepage: www.elsevier.com/locate/energy

Micro Newcomen steam engine using two-phase working fluid

Yang Wang, Zhijun Zhou*, Junhu Zhou, Jianzhong Liu, Zhihua Wang, Kefa Cen

State Key Laboratory of Clean Energy Utilization, Zhejiang University, Hangzhou 310027, Zhejiang, China

ARTICLE INFO

Article history:
Received 4 March 2010
Received in revised form
8 December 2010
Accepted 11 December 2010
Available online 21 January 2011

Keywords:
Ripple tube
Micro scale
Newcomen steam engine
Thermodynamic cycle

ABSTRACT

A micro steam engine is developed based on Newcomen steam engine. In the micro engine, a flexible ripple tube takes the place of piston and cylinder, to overcome the serious problems of friction and leakage in micro scale. We use two-phase octane as working fluid of the micro engine, because two-phase octane has higher power density than gaseous one. The micro engine is tested under different operational conditions to investigate its performance. It produces a maximum net mechanical work of 0.405 J per cycle with an efficiency of 2.58%. This experiment proves the feasibility of the micro steam engine.

1. Introduction

The power of portable electronic devices, such as laptops, cellular phones, is supplied by battery. Its energy densities are less than 0.5 MJ/kg [1], thus limit the operation period. Micro power system converts chemical energy of hydrocarbon fuels to electricity directly, thus has higher power density [2]. Its performance will excel the conventional battery, if only its efficiency is higher than 1% [3–5]. Although fuel cells have higher efficiency than micro power system [6]. They are made of expensive Pt material and only adapt a few kinds of fuel with high purity.

The first micro gas turbine based on Micro Electro Mechanical System (MEMS) technology was suggested in Massachusetts Institute of Technology (MIT) in 1996 [7]. Then, Jan Peirs developed a single-stage axial micro turbine driven by compressed air [1]. Besides micro turbine, internal combustion micro engine was also proposed [8]. For example, C.H. Lee produced a micro Wankel engine driven by CO_2 [9]. Zhang Shimin fabricated a prototype of micro free-piston swing engine [10]. Homogeneous Charge Compression Ignition (HCCI) was also proposed to improve the micro engine's performance [11–13]. To overcome the serious problems of friction and leakage between mechanical parts in micro engine [14], T. Geng fabricated a micro pulsejet [15]. S. Whalen developed a novel P3 engine, made of an elastic membrane [16,17]. Energy converters based on thermoelectric or thermophotovoltaic material were also proposed [2,18–20].

Technology of manufacture limits the development of micro engine. The low machining accuracy causes friction and abrasion of the mechanical parts. The leakage also induces low efficiency. These problems cause poor performance and instability of micro engine [1].

In this paper, a new micro steam engine is proposed. We try to take the place of piston and cylinder of engine with a flexible ripple tube. It works as one monolithic part, thus solves the problems of friction and leakage. In the experiment, we test the micro engine prototype under different operational conditions, to prove its feasibility.

2. Experimental system

2.1. Experimental facility

The prototype engine is developed based on Newcomen steam engine. For experimental convenience, the engine is powered by electricity instead of fuel. A block diagram of the facility is shown in Fig. 1. The experimental system has a loader and a heater installed, which exchange mechanical energy and heat with the engine, respectively.

The loader consists of a weight, an AC motor and a linear sensor (WS KTR-50). The motor lifts and drops the weight to change the pressure inside the ripple tube. A linear sensor monitors the displacement of ripple tube top.

The boiler has dimensions of 25 × 45 × 52 mm. The heater is a 160-W electrical heating tube installed into it. It is turned on and off to change the temperature of working fluid. A K-type thermal

* Corresponding author. Tel./fax: +86 571 87951616.
E-mail address: zhouzj@cmee.zju.edu.cn (Z. Zhou).

0360-5442/$ – see front matter © 2010 Elsevier Ltd. All rights reserved.
doi:10.1016/j.energy.2010.12.019

Nomenclature

η	efficiency
ΔT	temperature difference of thermodynamic cycle [K]
T_{hot}	high temperature of thermodynamic cycle [K]
W	mechanical work output per cycle [J]
p	pressure [kPa]
T	temperature [K]
s	entropy [J/K·kg]
W_{heat}	mechanical work output during heating [J]
W_{out}	total mechanical work output [J]
W_{ex}	mechanical work output during expansion [J]
W_{cool}	mechanical work input during cooling [J]
W_{in}	total mechanical work input [J]
W_{com}	mechanical work input during compression [J]
W_{net}	net mechanical work output per cycle [J]
Q	heat absorption per cycle [J]
Q_{in}	heat absorption during heating [J]
Q_{net}	net heat absorption per cycle [J]
C_v	specific heat at constant volume [J/kg K]
Q_{out}	heat loss to environment during cooling [J]
V	volume [m^3]
v''	specific volume of saturated vapor [m^3/kg]
v'	specific volume of saturated liquid [m^3/kg]
p_s	saturation pressure [kPa]
T_s	saturation temperature [K]
C_p	constant pressure heat capacity [J/kg K]
ρ	fluid density [kg/m^3]
m	mass of working fluid [kg]
m_{gas}	mass of gas [kg]
x	displacement [mm]
Δh	latent heat for vaporization [J]

couple and a diffuse silicon piezoelectric pressure sensor (AOB-131) monitor the temperature and pressure inside, respectively.

A digital data acquisition device (WSP-D806) collects the temperature signal. The pressure and displacement signals are transmitted to the analog input model (I7017). A digital output model (I7050D) controls the switch of loader and heater. All the signals are controlled or monitored by the computer.

The ripple tube is made of stainless steel. It expands and shrinks alternatively to produce mechanical work. A photograph of the ripple tube is shown in Fig. 2. For the convenience of manufacture, assembling and measurement, we use the ripple tube with centimeter-scale in the preliminary experiment. It has dimensions of $\varphi 46 \times 41$ mm and thickness around 0.2 mm.

The engine utilizes two-phase octane as its working fluid [21]. Octane is chosen because of its lower latent heat for vaporization (Δh). According to Clausius–Clapeyron Equation and Carnot equation (Eqs (1)and (2)), while the pressure difference is limited, lower Δh induces higher temperature difference of thermodynamic cycle (ΔT), thus increases the efficiency. Moreover, two-phase octane has higher mechanical work output per cycle. According to Eq (3), while ΔT and volume (V) are fixed, the mechanical work output per cycle (W) is proportional to the density (ρ) and heat capacity (C_p) of working fluid. Saturated liquid octane has ρ and C_p of 700 kg/m^3 and 2293 J/kg K [22], respectively, much higher than gaseous octane (4.97 kg/m^3 and 2092 J/kg K) [23].

$$\frac{\mathrm{d}\, p_s}{\mathrm{d}\, T_s} = \frac{\Delta h}{T_s(v'' - v')} \tag{1}$$

$$\eta = \frac{\Delta T}{T_{hot}} \tag{2}$$

$$W = \eta \cdot \Delta T \cdot \rho \cdot C_p \cdot V \tag{3}$$

2.2. Operation process

The control system switches the on/off of heater and loader alternatively, using the displacement of the ripple tube top (x) as a benchmark. The operation process of micro engine is shown in Fig. 3. A, during heating, the ripple tube expands from its initial displacement (x_0). Once the displacement reaches certain value (x_1), the weight is lifted and heater is turned off simultaneously. B, the expansion starts. C, the residual heat of octane is lost into the environment through passive natural convective cooling. Corresponding shrink makes the displacement decreases. When it

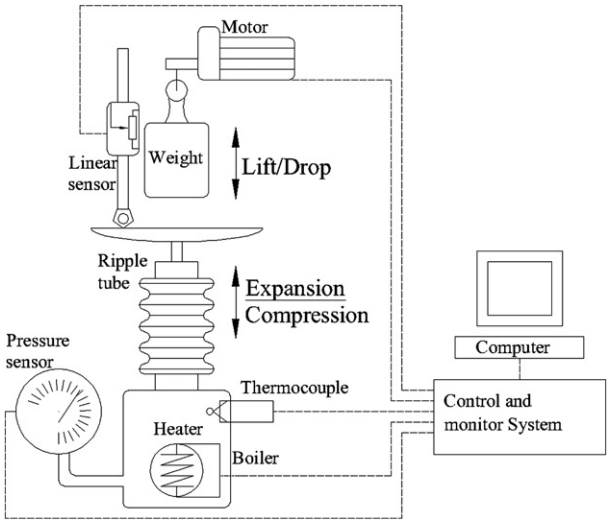

Fig. 1. Experimental system of the micro engine. The dashed lines are the signal routes.

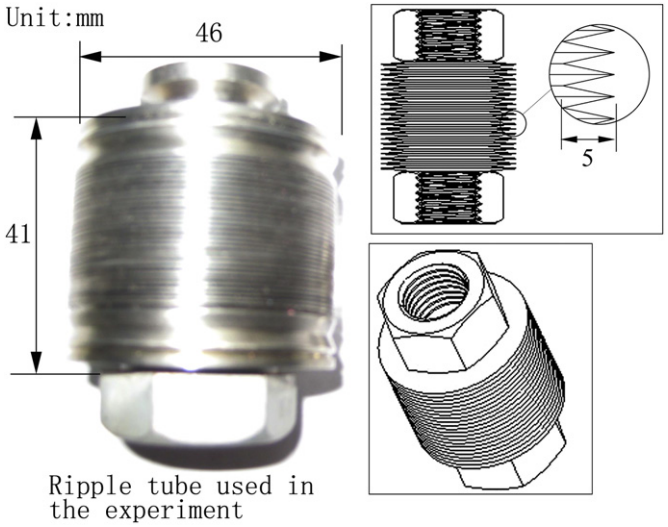

Fig. 2. Photograph of ripple tube.

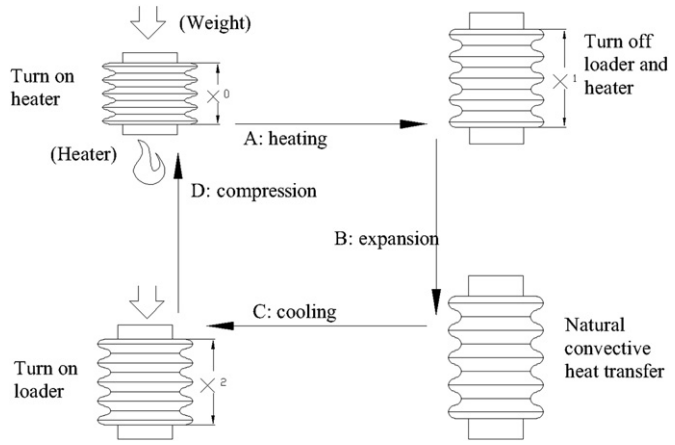

Fig. 3. Operation process of the micro engine. x is the displacement of the top of ripple tube.

reaches certain lower value (x_2), the loader is switched on. D, the weight compresses the octane to the initial condition. The thermodynamic cycle completes.

The engine is tested under different expansion volume and pressure, which would affect its thermodynamic cycle. The expansion volume is adjusted through changing the critical displacement for switching heater or loader. The pressure is adjusted through changing the mass of weight. The parameters of different operational conditions are listed in Table 1.

2.3. Calculation

In the experiment, part of the octane remains as liquid and does not expand or shrink during the thermodynamic cycle. Thus only the octane doing mechanical work is analyzed. The parameters of entropy (s), volume (V), temperature (T) and pressure (p) depict the thermodynamic cycle, and derive the net mechanical work output (W_{net}), net heat absorption (Q_{net}), internal energy (E) and efficiency (η).

In this experiment, natural convective cooling is inefficient and prolongs the period of thermodynamic cycle, which induces low power output [24]. Therefore, the data of power is invalid, and the net mechanical work output per cycle is analyzed instead, shown as Eq. (4).

$$W_{net} = \int pV \tag{4}$$

The net heat absorption equals to the difference of internal energy (ΔE) subtracting the net mechanical work output, shown as Eq. (5).

$$Q_{net} = \Delta E - W_{net} \tag{5}$$

The internal energy of two-phase octane is calculated with Eq. (6). m is the mass of working fluid. C_v is the specific heat at constant volume. m_{gas} is the mass of gas. Δh is the latent heat for vaporization. T is the temperature.

$$E = mC_vT + m_{gas}\Delta h \tag{6}$$

The entropy is calculated with Eq. (7).

$$s = \frac{Q}{T} \tag{7}$$

The efficiency is defined as Eq. (8). W_{net} is the net mechanical work output. Q_{in} is the total heat absorption.

$$\eta = \frac{W_{net}}{Q_{in}} \tag{8}$$

The error in calculation is analyzed. The independent parameters measured in the experiments are: T, p and x. Errors of T and p are both 0.5%, and error of x is 0.05%, according to the instruction of instruments. Error of the dimension of ripple tube is less than 1%. Conclusively, the maximum possible uncertainties of W_{net}, Q_{net}, E, s and η are 2.1%, 2.3%, 2.4%, 1.8% and 0.24%, respectively.

Table 1
Parameters of operational conditions in different cases. x is marked in Fig. 3, which indicates the critical displacement for switching loader or heater.

Case	Mass of weight (kg)	x_0 (mm)	$x_1 - x_0$ (mm)	$x_2 - x_0$ (mm)
1	0.5	33	5	2
2	0.5	38	5	2
3	0.5	33	10	2
4	1	33	5	2
5	1	38	5	2
6	1	33	10	2

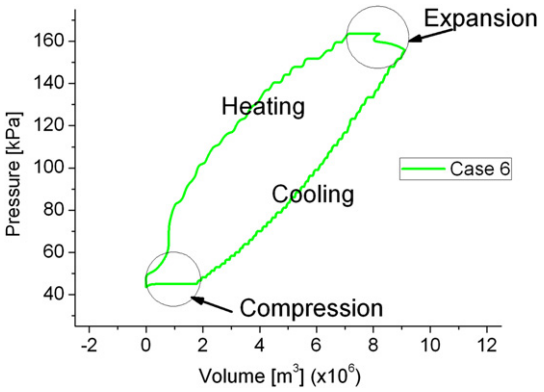

Fig. 4. Volume–pressure curve of the thermodynamic cycle in Case 6.

3. Results and discussion

3.1. Typical thermodynamic cycle

Fig. 4 shows a typical volume–pressure diagram of Case 6 in Table 2. The maximum pressure and volume are 163 kPa and 9.26×10^{-6} m^3, respectively. Fig. 5 shows the according entropy–temperature profile. The peak temperature of the thermodynamic cycle reaches 417 K, which is much lower than conventional thermodynamic cycle. It has negative effects to the efficiency. Working fluid with higher boiling point may improve it.

The thermodynamic cycle composes of four processes: heating, expansion, cooling and compression. During heating both the volume and pressure increase. The flexibility of ripple tube makes the pressure increase with expansion volume, thus makes heating process a polytropic process. According to Fig. 5, the temperature increases with pressure simultaneously, which slims the

Table 2
Total heat absorption, net mechanical work output and efficiency in different cases.

Case	Q_{in} [J]	W_{net} [J]	η
1	10.1	0.193	1.91%
2	8.7	0.175	2.00%
3	15.6	0.306	1.97%
4	9.6	0.227	2.37%
5	9.5	0.232	2.44%
6	15.7	0.406	2.58%

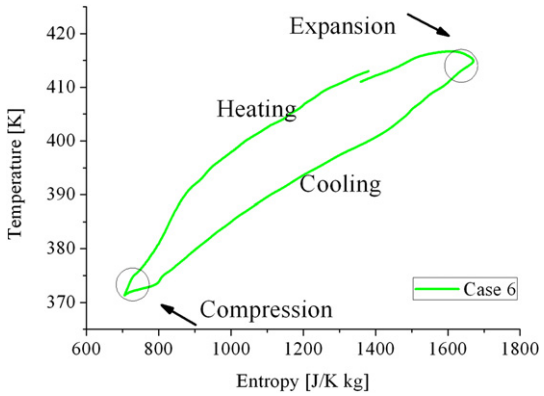

Fig. 5. Entropy–temperature curve of the thermodynamic cycle in Case 6.

thermodynamic cycle, thus decreases the efficiency and mechanical work output.

Note that the pressure stays almost the same during expansion. It is because that the thermal inertia of working fluid increases dramatically in micro scale, which makes the temperature change more slowly. As a consequence, the pressure, which is related to temperature in two-phase condition, decreases slightly during expansion.

During cooling, the ripple tube shrinks with the octane inside. The pressure also decreases with the volume. Finally, in the compression process, the pressure stays almost the same as the volume decreases. The reason is similar as the expansion process.

3.2. Comparison of different cases

The pressure–volume curves and entropy–temperature curves in Case 1, 2, 3 are shown in Figs. 6 and 7, respectively. Take Case 3 as an example, at the maximum expansion volume of 8.06×10^{-6} m^3, the pressure reaches the peak value of 144 kPa. Simultaneously, the working fluid has its temperature increase to 413 K, and the entropy increase to 1618 J/K kg. The dot line delineates the saturation state of octane calculated by Eq. (9) [25]. According to the saturation line, octane keeps as two-phase fluid during the thermodynamic cycle. The net mechanical work output, total heat absorption and derived efficiency in different cases are summarized in Table 2.

$$\log_{10} p_s = 4.04867 - \left(\frac{1355.126}{T_s - 63.633}\right) \tag{9}$$

The efficiencies in Case 1, 2 and 3 are around 2%. The net mechanical work output in Case 3 reaches 0.306 J, exceeding 0.193 J

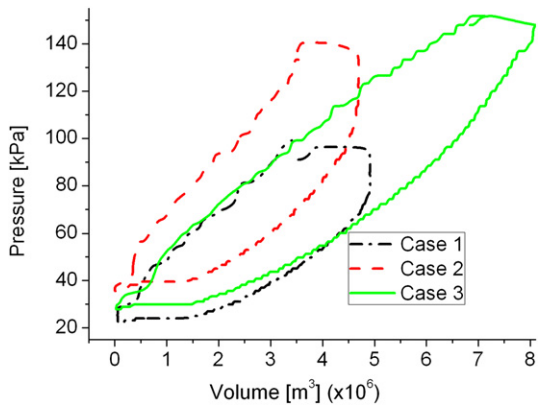

Fig. 6. Volume–pressure curves of the thermodynamic cycle in Case 1, 2 and 3.

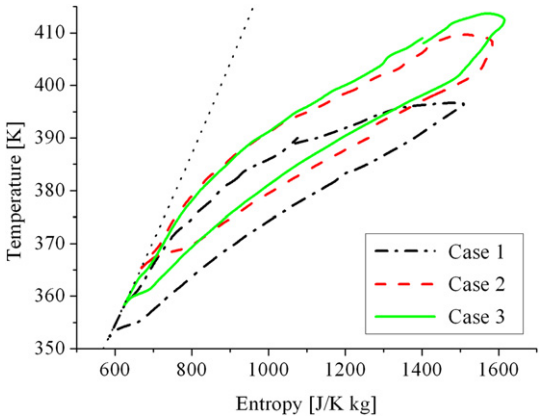

Fig. 7. Entropy–temperature curves of the thermodynamic cycle in Case 1, 2 and 3.

in Case 1. The maximum expansion volumes of Case 3 and 1 are 8.06×10^{-6} m^3 and 5.32×10^{-6} m^3, respectively. Accordingly, the thermodynamic curve of Case 3 envelops a larger area than Case 1. Therefore, it shows a higher net mechanical work output. The results prove that it is feasible to improve the engine's performance through increasing its expansion volume.

However, the expansion volume of ripple tube is limited. Experiment is conducted to find other ways for improvement, for example, increase the mass of weight [26]. The pressure–volume curves and entropy–temperature curves in Cases 4, 5 and 6 with the weight of 1 kg are shown in Figs. 8 and 9, respectively. The efficiencies are around 2.4% according to Table 3. Compared with the previous three cases with weight of 0.5 kg, it proves that the efficiency increases with mass of weight. The primary reason is that the heavier weight increases the maximum pressure of the thermodynamic cycle, thus enlarges the temperature difference accordingly (temperature is related to pressure in two-phase condition). The minimum and maximum temperatures in Case 3 and 6 are 382–401 K and 384–415 K, respectively. Therefore, the efficiency increases according to the second thermodynamic law [27]. The higher efficiency increases the net mechanical work output consequently. The net mechanical work output in Case 6 is 0.1 J higher than Case 3.

3.3. Mechanical work distribution

The distribution of mechanical work throughout the thermodynamic cycle is analyzed. During heating, heat (Q_{in}) is transferred to octane, and octane also has mechanical work output (W_{heat}).

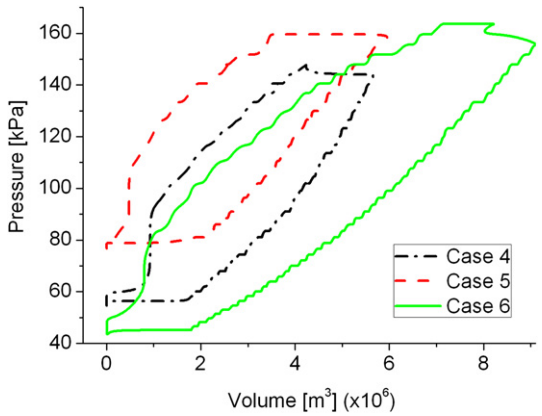

Fig. 8. Volume–pressure curves of the thermodynamic cycle in Case 4, 5 and 6.

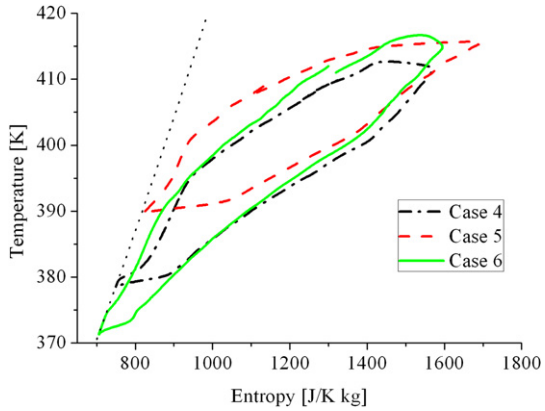

Fig. 9. Entropy–temperature curves of the thermodynamic cycle in Case 4, 5 and 6.

Table 3
Fractions of the mechanical work output and input during different sections of the thermodynamic cycle.

Case	W_{heat}/W_{out}	W_{ex}/W_{out}	W_{cool}/W_{in}	W_{com}/W_{in}
1	62.1%	37.9%	84.1%	15.9%
2	67.3%	32.7%	77.4%	22.6%
3	77.7%	22.3%	91.8%	8.2%
4	67.3%	32.7%	76.4%	23.6%
5	62.9%	37.1%	72.4%	27.6%
6	74.2%	25.8%	90.7%	9.3%

During expansion, octane does mechanical work (W_{ex}). During cooling, heat (Q_{cool}) is lost into the environment, and octane has mechanical work input (W_{cool}). During compression, the mechanical work input (W_{com}) returns the octane to its initial condition.

Table 3 shows the fractions of mechanical work output and input during different sections of the thermodynamic cycle. W_{in} and W_{out} are the total mechanical work input and output, respectively. In all the six cases, the mechanical work output during expansion occupies a relatively small fraction of the total mechanical work output. Take Case 6 as an example, during heating and expansion, the octane has a total mechanical work output of 1.19 J. Its fractions during heating and expansion are 74.2% and 25.8%, respectively.

The conventional thermodynamic cycle has the mechanical work output mainly during expansion. However, in the micro engine, most of the mechanical work is produced during heating instead of expansion, due to the flexibility of ripple tube. It prevents the octane from reaching higher peak temperature during heating, thus decreases the efficiency and mechanical work output. Conclusively, higher fraction of mechanical work output during expansion will improve the performance of micro engine.

4. Conclusion

A micro steam engine using two-phase octane as working fluid has been tested. According to the experimental results, the micro engine generates a net mechanical work output of 0.406 J per cycle in the maximum.

The micro engine has the highest efficiency of 2.58%, which exceeds the required level (1%) of micro engine [1]. Therefore, the experiment proves its feasibility. But the micro engine requires improvement for better performance. It is possible through optimizing the operational parameters.

References

[1] Peirs J, Reynaerts D, Verplaetsen F. A microturbine for electric power generation. Sensors and Actuators A: Physical 2004;113(1):86–93.
[2] Ahn J, Eastwood C, Sitzki L, Ronney PD. Gas-phase and catalytic combustion in heat-recirculating burners. Proceedings of the Combustion Institute 2005;30 (2):2463–72.
[3] Jacobson SA, Epstein AH. An information survey of power MEMS. The International Symposium on micro-mechanical engineering. Tsukuba, Japan; 2003.
[4] Fernandez-Pello AC. Micro-power generation using combustion: issues and approaches. Twenty-Ninth International Symposium on combustion. The Combustion Institute; 2002; Sapporo, Japan; 2002. p. 1–45.
[5] Spadaccini CM, Mehra A, Lee J. High power density silicon combustion system for micro gas turbine. Journal of Engineering for Gas Turbines and Power 2003;9(4):517–27.
[6] Peacock AD, Newborough M. Impact of micro-combined heat-and-power systems on energy flows in the UK electricity supply industry. Energy 2006;31 (12):1804–18.
[7] Epstein AH, Senturia SD, Anathasuresh G, Ayon A, Breuer K, Chen K-S, et al. Power MEMS and microengines. IEEE Transducers' 97 Conference; 1997; Chicago; 1997.
[8] Suzuki Y, Okada Y, Ogawa J, Sugiyama S, Toriyama T. Experimental study on mechanical power generation from MEMS internal combustion engine. Sensors and Actuators A: Physical 2008;141(2):654–61.
[9] Lee CH, Jiang KC, Jin P, Prewett PD. Design and fabrication of a micro Wankel engine using MEMS technology. Microelectronic Engineering 2004;73-74:529–34.
[10] Zhang S, Wang J, Guo Z. Novel micro free-piston swing engine and its feasibility validation. Tsinghua Science & Technology 2005;10(3):381–6.
[11] Aichlmayr HT, Kittelson DB, Zachariah MR. Micro-HCCI combustion: experimental characterization and development of a detailed chemical kinetic model with coupled piston motion. Combustion and Flame 2003;135 (3):227–48.
[12] Aichlmayr TH, Kittelson BD, Zachariah RM. Miniature free-piston homogeneous charge compression ignition engine-compressor concept–part II: modeling HCCI combustion in small scales with detailed homogeneous gas phase chemical kinetics. Chemical Engineering Science 2002;57 (19):4173–86.
[13] Aichlmayr HT, Kittelson DB, Zachariah MR. Miniature free-piston homogeneous charge compression ignition engine-compressor concept–part I: performance estimation and design considerations unique to small dimensions. Chemical Engineering Science 2002;57(19):4161–71.
[14] Sher I, Levinzon-Sher D, Sher E. Miniaturization limitations of HCCI internal combustion engines. Applied Thermal Engineering 2009;29(2–3):400–11.
[15] Geng T, Zheng F, Kiker AP, Kuznetsov AV, Roberts WL. Experimental and numerical investigation of an 8-cm valveless pulsejet. Experimental Thermal and Fluid Science 2007;31(7):641–7.
[16] Cho J-H, Lin CS, Richards CD, Richards RF, Ahn J, Ronney PD. Demonstration of an external combustion micro-heat engine. Proceedings of the Combustion Institute 2009;32(2):3099–105.
[17] Whalen S, Thompson M, Bahr D, Richards C, Richards R. Design, fabrication and testing of the P3 micro heat engine. Sensors and Actuators A: Physical 2003;104(3):290–8.
[18] Yang WM, Chou SK, Shu C, Xue H, Li ZW, Li DT, et al. Microscale combustion research for application to micro thermophotovoltaic systems. Energy Conversion and Management 2003;44(16):2625–34.
[19] Wenming Y, Siawkiang C, Chang S, Hong X, Zhiwang L. Effect of wall thickness of micro-combustor on the performance of micro-thermophotovoltaic power generators. Sensors and Actuators A: Physical 2005;119(2):441–5.
[20] Yang WM, Chou SK, Shu C, Li ZW, Xue H. Experimental study of micro-thermophotovoltaic systems with different combustor configurations. Energy Conversion and Management 2007;48(4):1238–44.
[21] Kim KB, Choi KW, Kim YJ, Lee KH, Lee KS. Feasibility study on a novel cooling technique using a phase change material in an automotive engine. Energy 2010;35(1): 478–84.
[22] Garg SK, Banipal TS, Ahluwalia JC. Heat capacities and densities of liquid n-octane, n-nonane, n-decane, and n-hexadecane at temperatures from 318.15 to 373.15 K and at pressures up to 10 MPa. Chemical Thermodynamics 1991;23:923–31.
[23] Hossenlopp IA, Scott DW. Vapor heat capacities and enthalpies of vaporization of five alkane hydrocarbons. Chemical Thermodynamics 1981;13:415–21.
[24] Kaushik SC, Kumar S. Finite time thermodynamic analysis of endoreversible Stirling heat engine with regenerative losses. Energy 2000;25(10):989–1003.
[25] Williamham CB, Taylor WJ, Pignocco JM, Rossini FD. Vapor pressures and boiling points of some paraffin, alkylcyclopentane, alkylcyclohexane, and alkylbenzene hydrocarbons. Journal of Research of the National Bureau of Standards 1945;35:219–44.
[26] Timoumi Y, Tlili I, Ben Nasrallah S. Design and performance optimization of GPU-3 Stirling engines. Energy 2008;33(7):1100–14.
[27] Hongqing F, Huijie L. Second-law analyses applied to a spark ignition engine under surrogate fuels for gasoline. Energy 2010;35(9): 3551–56.